

Depletion zones and crystallography on pinched spheres

Jingyuan Chen^{1,2}, Xiangjun Xing^{1,3} and Zhenwei Yao^{1,2*}

¹*School of Physics and Astronomy, and* ²*Institute of Natural Sciences, Shanghai Jiao Tong University, Shanghai 200240 China*

³*Collaborative Innovation Center of Advanced Microstructures, Nanjing 210093, China*

Understanding the interplay between ordered structures and substrate curvature is an interesting problem with versatile applications, including functionalization of charged supramolecular surfaces and modern microfluidic technologies. In this work, we investigate the two-dimensional packing structures of charged particles confined on a pinched sphere. By continuously pinching the sphere, we observe cleavage of elongated scars into pleats, proliferation of disclinations, and subsequently, emergence of a depletion zone at the negatively curved waist that is completely void of particles. We systematically study the geometrics and energetics of the depletion zone, and reveal its physical origin as a finite size effect, due to the interplay between Coulomb repulsion and concave geometry of pinched sphere. These results further our understanding of crystallography on curved surfaces, and have implications in design and manipulation of charged, deformable interfaces in various applications.

I. INTRODUCTION

Electrically charged and deformable interfaces are widely seen in natural and synthetic two-dimensional systems, ranging from charged droplets of spherical [1–3], cylindrical [4, 5] and toroidal [6, 7] geometries, various charged elastic ribbons fabricated by supramolecular self-assembly [8, 9] to charged lipid membranes [10–12]. Surface charges can strongly affect morphologies of deformable interfaces [13–16], renormalize their elastic rigidities [17–20], and create local electrostatic structures with chemical and biological implications [9, 12]. Proper understanding of the subtle interplay between long-range Coulomb interaction and surface morphology is not only interesting from a theoretical point of view, but also a prerequisite for applications of charged deformable interfaces, including morphology-based functionalization of charged supramolecular surfaces [9, 21, 22] and modern microfluidic technologies involving electrostatic dispersion of liquids [23–27]. As a classic example, Lord Rayleigh demonstrated that Coulombic repulsion drives large deformation and fission of a charged liquid droplet long ago [1].

Another interesting example is the Thomson problem [28–32], which is to find the ground state of charged particles confined on a spherical surface. In the resulting triangular lattice on the sphere, several curvature-driven crystallographic defect motifs like scars [33] and vacancies [34, 35] have been discovered in the extensive theoretical [36–41] and experimental [33, 34, 42, 43] studies. By allowing the surface to be deformable, the generalized Thomson problem can be employed to explore the coupling of charged particles distribution and the deformation of the interface. This can be experimentally realized by depositing electrically charged colloids at the spherical water-oil interface [33, 42], or by encapsulating

an aqueous mixture of colloids of different sizes within spherical water-in-oil droplets [34].

In this work, we shall control the deformation of interface, and study the lowest-energy distribution of the charges that are mobile on the surface. Specifically, we pinch a sphere around the equator to form a peanut-like shape. The pinching creates a negatively curved region near the waist. Our study shows that this has strong influence on the packing structure of charges, leading to formation of the elongated scars which further evolve into pleats, as well as formation of cracks that ultimately evolve to a depletion zone, where all charges are excluded.

We systematically study the geometric structure of the depletion zone, and demonstrate that it is a robust feature of the lowest-energy states, resulting from the interplay between Coulombic repulsion and the concave geometry of the waist. Furthermore, heuristic arguments in terms of continuum electrostatics show that the depletion zone structure is a finite size effect. Finally, we briefly discuss packing of charges on a biconcave discoidal shape, and find similar defect patterns and depletion zones. The discovery of depletion zone structure over the concave geometry enriches our understanding of the crystallographic defects in curved crystals, and may have useful applications in the design and manipulation of charged deformable interfaces.

II. MODEL AND METHOD

A pinched sphere can be described in terms of the spherical harmonics as

$$r(\theta) = R [1 + \kappa(3 \cos^2 \theta - 1)], \quad (1)$$

where θ is the polar angle, and κ is a dimensionless parameter controlling the degree of pinching. For $0 < \kappa < 1$, the pinched sphere exhibits a peanut-like shape, as illustrated in Fig. 1. The radius achieves minimum at the *waist*, with $r(\theta = \pi/2) = (1 - \kappa)R$, which shrinks as κ in-

*Electronic address: zyao@sjtu.edu.cn

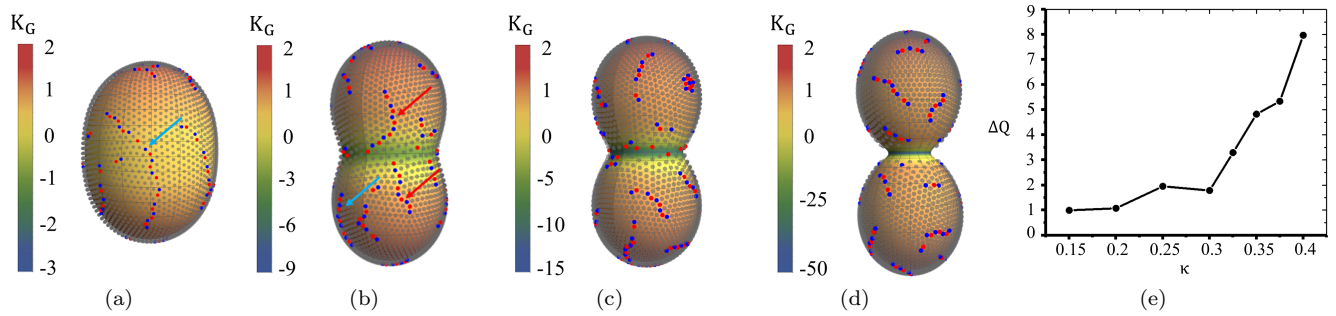


FIG. 1: Lowest-energy particle configurations over the typical pinched spheres. The degree of the pinching deformation is characterized by κ . (a) $\kappa = 0.1$, (b) 0.3, (c) 0.4, and (d) 0.6. The five- and seven-fold disclinations are colored in red and green, respectively. The rightmost panel shows the distribution of the mean curvature. (e) Plot of the excess topological charge ΔQ in the waist region over the pinched sphere versus κ . $N = 3000$.

creases. For $-1/2 < \kappa < 0$, the pinched sphere becomes a biconcave discoid, illustrated in Fig. 5.

The Gaussian curvature [44] of a surface is given by

$$K_G = 1/R_1 R_2, \quad (2)$$

where R_1 and R_2 are two radii of principal curvatures. For a pinched sphere Eq. (1), the Gaussian curvature is

$$K_G = -\frac{1}{2\sqrt{|g|}} \frac{\partial}{\partial \theta} \left(\frac{1}{\sqrt{|g|}} \frac{\partial}{\partial \theta} (r^2 \sin^2 \theta) \right). \quad (3)$$

where $|g|$ is the determinant of the metric tensor. For $\kappa > 0$, K_G reaches minimum at the waist circle $\theta = \pi/2$:

$$K_{G,\min} = \frac{1 - 7\kappa}{(1 - \kappa)^3}. \quad (4)$$

$K_{G,\min}$ becomes zero when $\kappa = 1/7$, and diverges as $\kappa \rightarrow 1$. Hence, for $1/7 < \kappa < 1$, the waist area is negatively curved. According to the Gauss-Bonnet-Chern theorem[45], the integral of the Gaussian curvature over a smooth surface of spherical topology is 4π , which is a topological invariant.

We perform simulations to find the lowest-energy state of a collection of point charges confined on the pinched sphere Eq. (1). These charges interact with each other via the three-dimensional Coulomb potential $V_{ij} \sim 1/r_{ij}$, where r_{ij} is the distance between particle i and j . We find the lowest-energy state by starting from a random initial state (unless specified otherwise) and let the particles move incrementally along the forces acting on them. We update the particle configuration in a collective manner to rapidly reduce the system energy, followed by moving individual particles in each simulation step to fine tune the system down to the bottom of the energy surface. This protocol has been applied in several charged particle systems and has successfully generated lowest-energy states [16, 46].

In Fig. 2(a) and 2(b), we show the reduction of system energy towards the lowest value for the cases of $\kappa = 0.15$ and $\kappa = 0.71$, respectively. $\delta\tilde{E} = (E_e - E_f)/E_f$, where

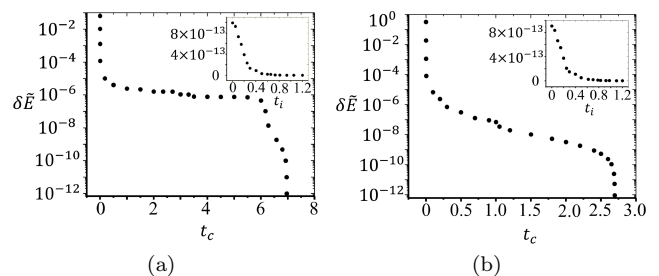


FIG. 2: Convergence of system energy towards the lowest value for the cases of (a) $\kappa = 0.15$ and (b) $\kappa = 0.71$. $\delta\tilde{E} = (E_e - E_f)/E_f$, where E_e is the total electrostatic energy and E_f is that in the lowest energy state. In the collective movement of particles, step size is gradually reduced to accelerate energy reduction. The unit of t_c is 10000 sweeps over all the particles, and that of t_i in the individual mode (shown in the insets) is by sweeping 10000 particles. $N = 3000$.

E_e is the total electrostatic energy and E_f is that in the lowest energy state. The unit of t_c is 10000 sweeps over all the particles. In the collective movement of particles, we gradually reduce the step size from $2a_0$ to $7.8 \times 10^{-4} a_0$ for efficiency in energy reduction. a_0 is the lattice spacing. We further reduce system energy by moving particles individually, and the results are presented in the insets in Fig. 2. We see that the system energy rapidly converges after a few sweeps. Note that the unit of t_i in the individual mode is by sweeping 10000 particles.

We analyze the crystallographic defects in the resulting lowest-energy states using the method of Delaunay triangulation [29]. While this is a standard procedure of triangulation on plane, the existence and uniqueness of triangulated state using this method on a negatively curved surface is not guaranteed. To solve this problem, we choose a disk-shape neighborhood of each particle, and project it on to the tangent plane. As long as the disk radius is sufficiently small, the curvature within the disk can be ignored. By performing the standard Delaunay triangulation over these particles projected to the plane, we can determine the coordination number of each

particle without unambiguity.

To check the validity of our simulation codes, we first simulate the evolution of charged particles on an unperturbed spherical substrate. Starting from an initial state with dense distribution of disclinations, we numerically observe the annihilation of disclinations. Only a few scattered scars and dislocations survive in the final lowest-energy states that our simulations can reach. These observations are consistent with the known results in spherical crystals, suggesting the reliability of our simulations.

III. RESULTS AND DISCUSSION

A. From elongated scars to pleats

Past experimental [33] and theoretical [37] studies have established that the charges confined on a sphere will spontaneously organize into a triangular lattice, with various sorts of defects [29, 31, 32], including disclinations, dislocations and scars. A z -fold vertex, i.e. a particle with coordination number z , is called a disclination if z differs from six. The topological charge of a disclination is defined as $q = (6 - z)\pi/3$. According to Euler's theorem [44], the total topological charge of a spherical crystal is a topological invariant: $\sum_i q_i = 4\pi$, where the sum is over all particles of lattice. A dislocation is a pair of five- and seven-fold disclinations, with vanishing net topological charge. A scar is a string of alternating five- and seven-fold disclinations with two five-fold disclinations at the ends. The topological charge of a scar is hence $\pi/3$, the same as a single five-fold disclination. A scar is essentially a grain boundary across which a mismatch of crystallographic orientation occurs.

It has been established by previous studies that in a sufficiently large spherical crystal, the isolated point-like five-fold disclinations become unstable and crack into scars [33]. The length of the scars is determined by the ratio R/a , where R is the spherical radius, while a is the lattice spacing. By slightly pinching the sphere along its equator, we observe an appreciable change of scar lengths. Elongated scars are found over the pinched spherical crystal, as indicated by the blue arrow in Fig. 1(a). These scars tend to align along the long axis (defined as the z -axis) of the pinched sphere.

When κ increases to about 0.3, we find strings of alternating disclinations with a five-fold disclination at one end and a seven-fold disclination at the other end, as indicated by the red arrows in Fig. 1(b). Such defect strings are called *pleats*. Their net topological charge is zero [42]. Pleats have been first observed in the crystalline order on negatively curved capillary bridges [42]. We notice that the negatively charged ends of the pleats, indicated by the red arrows in Fig. 1(b), are anchored at the negatively curved waist, while the positively charged end are located in the positively curved region. Tracking the evolution of defect patterns as we tune the pinching, we find that these two pleats were split out from the

same elongated scar. As a consequence of this splitting, the scar becomes significantly shorter. In this process, an extra short scar is emitted to the surrounding crystalline region to conserve the total topological charge.

Past studies have demonstrated that Gaussian curvature can be understood as uniform counter-charge background that screens the topological charges of disclinations [29]. From this perspective, it is useful to define the *geometric charge* Q_g of the waist area as the integral of the Gaussian curvature, the *excess charge* ΔQ as $\Delta Q = Q_d - Q_g$, where Q_d is the total disclination charge. Figure 1(e) shows that the excess charge ΔQ is always positive over the range of $\kappa \in [0.15, 0.4]$, indicating that geometric curvature can only partially screen the topological defects. Furthermore, from Fig. 1(e), we see that ΔQ surges abruptly as κ increases from 0.3 to 0.4, which coincides with the emergence of pleats and complete disruption of crystalline order near the waist, as shown in Figs. 1(b) and 1(c). Previous studies have shown that long-range repulsion driven particle-density gradient will induce a negative Gaussian curvature and promote emergence of seven-fold disclinations [29, 47]. This effect may partially explain the excess topological charges in the waist area.

B. Depletion zone structure

Further increasing κ to 0.4, we observe filling of seven-fold disclinations and complete disruption of the crystalline order near the waist, as illustrated in Fig. 1(c). Concomitantly, the particle density near the waist also becomes much lower: this seems a favorable strategy to lower the electrostatic energy of the system. For $\kappa \geq 0.6$, we find the emergence of a sharply defined *depletion zone* (with no particle) around the waist, as shown in Fig. 1(d).

We shall verify that the depletion zone is a robust feature of the ground state. To this end, we start from initial states where only half of the pinched sphere ($\kappa = 0.7$) is occupied by randomly distributed particles. Once the dynamics is turned on, we find particles migrate to the other side through the waist. In the final lowest-energy state, a depletion zone is formed again over the waist region. The particle numbers at two sides of the waist differ by less than 1%. This indicates that the depletion zone is indeed a robust feature of the ground state and is independent of the initial condition.

We can also plot the electrostatic potential on the surface as a function of polar and azimuthal angle θ, ϕ . Figure 3(a) shows the case where particle numbers in the two sides of the waist are equal. It clearly shows that the potential has a maximum on the waist where $\theta = \pi/2$. A test charge (recall that all particles are positively charged) cannot be stabilized at the waist: it will move to either side. By contrast, Fig. 3(b) shows the case where particle numbers in two sides are slightly different (992 vs 1008 particles), and there is no potential maximum at the waist. The potential increases monotonically with the polar angle θ . A test charge placed

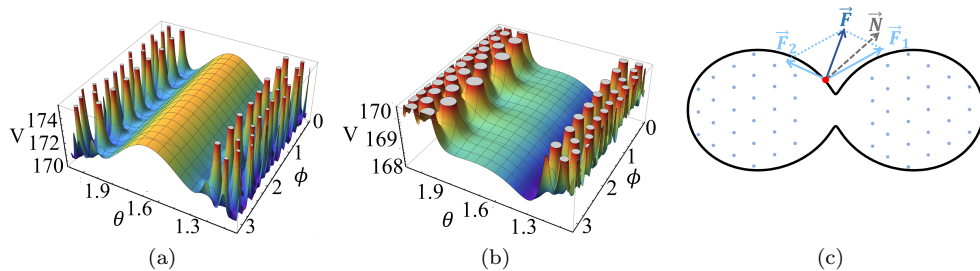


FIG. 3: The electric potential near the waist. θ, ϕ are polar and azimuthal angles, respectively. (a) Equal number of particles in two sides of the waist. There is a potential maximum on the waist. Hence a test charge cannot be stabilized near the waist. (b) Particle number in the two sides are slightly different. There is no potential barrier near the waist, and a test charge will automatically move to the right side with fewer particles. $\kappa = 0.7$. (c) Schematic plot of the force analysis on a test charge indicated by the red dot in the depletion zone (see text for more information).

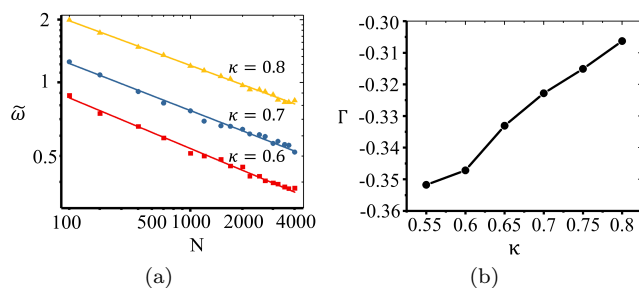


FIG. 4: Geometric characterization of the depletion zone structure in the lowest-energy pinched spherical crystals. (a) Logarithmic plot of the normalized width \tilde{w} of the depletion zone versus the number of particles N . The data can be well fitted by a power law with the exponent Γ . (b) Plot of Γ vs κ . $N = 3000$.

near the waist will move to the side with lower potential. These analyses further substantiate that the depletion zone is indeed a robust property of the ground state.

To better understand the potential maximum on the waist as shown in Fig. 3(a), let us consider the electrostatic force acting on a test charge slightly to the left of the waist, as schematically shown in Fig. 3(c). Since the test charge is confined on the surface, only the tangent component of the total force is relevant. Now, as the parameter κ increases, the waist becomes thinner, and the local normal vector \vec{N} rotates to the right. For sufficiently thin waist, \vec{N} is always to the right of \vec{F} , and hence the tangent component of \vec{F} always points to the left. That is, the test charge is pushed to the left. This is exactly what we see in Fig. 3(a). The depletion zone is caused by the local concave geometry near the waist.

We proceed to discuss the influence of particle number N and pinching parameter κ on the size of the depletion zone. Let \tilde{w} be the width of depletion zone normalized by the diameter of waist circle. Figure 4(a) shows that \tilde{w} shrinks as N increases, with the dependence well-described by a power law for N from 100 to 4000:

$$\tilde{w} \sim N^\Gamma. \quad (5)$$

where the exponent Γ increases linearly with κ , as shown in Fig. 4(b). This suggests that the depletion zone is a finite size effect, and will eventually disappear in the limit $N \rightarrow \infty$. Indeed, in this limit, we expect that the electrostatic potential is described by Laplace equation with *conductor boundary condition*, i.e., the potential is constant on the entire surface, since all charges are mobile in our model. Now if the charge density vanishes in certain region on the surface, then both the potential and its normal derivative are fixed. This corresponds to Cauchy boundary conditions, which is known to be incompatible with Laplace equation. We further note that since $|\Gamma| < 1/2$, \tilde{w} decays with N slower than the mean inter-particle distance $\langle a \rangle$, which scales as $1/\sqrt{N}$.

C. Negatively pinched sphere

It is also interesting to study the case of negative κ , where the surface has the shape of biconcave discoid. The defect structures for several negative values of κ are presented in Fig. 5. At $\kappa = -0.1$, we find scars [indicated by the blue arrow in Fig. 5(a)] around the rim of the pinched sphere where the Gaussian curvature reaches maximum, and pleats (indicated by the red arrow) over the slightly curved areas. At $\kappa = -0.2$, we find isolated seven-fold disclination at the dimple as shown in the inset of Fig. 5(b). Depletion zone starts to appear when κ is even more negative as shown Figs. 5(c) and 5(d) for the cases of $\kappa = -0.3$, and -0.4 . As in the case of positive κ , these depletion zones are expected to vanish in the limit $N \rightarrow \infty$.

D. Energetics analysis

So far, we have studied the packing of charged particles on frozen geometries. Many surfaces in realistic systems are deformable. Here, we track the variation of the total electrostatic energy as a function of the pinching parameter κ , following two protocols: (1)

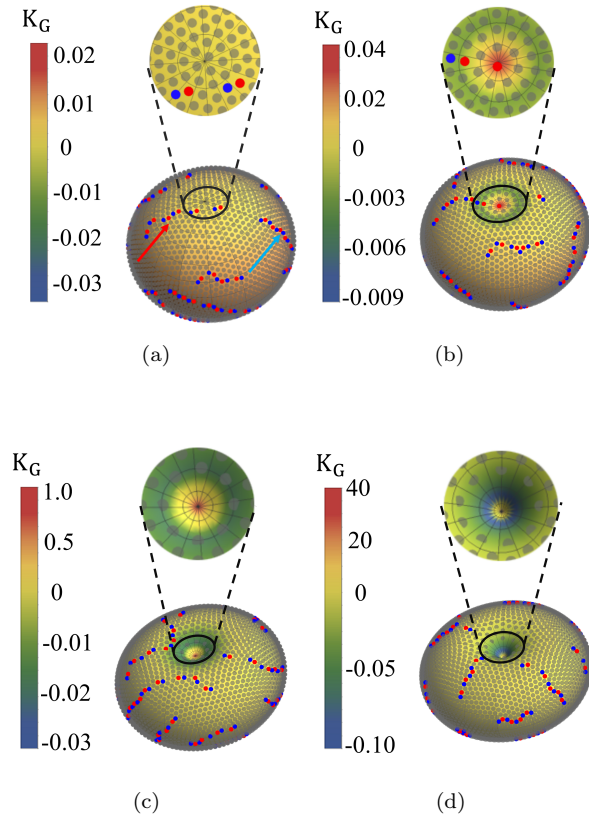


FIG. 5: Lowest-energy configurations on a pinched spheres with negative κ . (a) $\kappa = -0.1$, (b) $\kappa = -0.2$, (c) $\kappa = -0.3$, and (d) $\kappa = -0.4$. The five- and seven-fold disclinations are colored in blue and red, respectively. $N = 3000$.

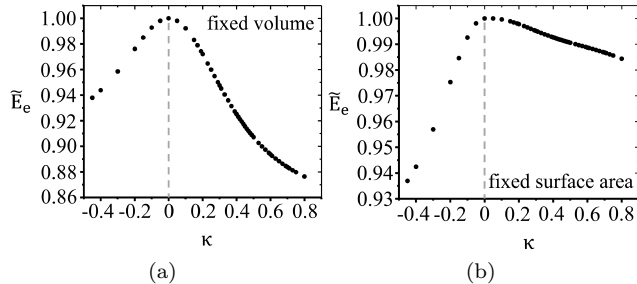


FIG. 6: Electrostatic energy as a function of pinching parameter κ normalized by its value at $\kappa = 0$. (a) Volume is fixed, but surface area changes with κ ; (b) Surface area is fixed, but volume changes with κ . $N = 3000$.

fixed volume [see Fig. 6(a)] and (2) fixed surface area [see Fig. 6(b)]. For both protocols, the total electrostatic energy decreases monotonously as κ deviate from zero. This indicates, rather interestingly, that the surface will

spontaneously deform to a non-spherical shape as long as the non-electrostatic interactions, such as surface tension and curvature energy, are sufficiently weak. This shall be discussed in a separate work. We also note that the reduction of the total electrostatic energy indicates that pinching a charged sphere can increase its capacitance as an electric conductor, since $C = Q/U = Q^2/(2E)$, where Q is the total charge, U is the electric potential, and E is the electrostatic energy of the conductor.

IV. CONCLUSION

In this work, the charged interface is deformed in a controllable fashion by tuning the single parameter κ . This strategy has its merit, but it inevitably excludes the possibilities of other lowest-energy shapes. Rich structures can be developed on a charged interface, such as the experimentally observed singularity structures developed at the poles of a charged ellipsoidal droplet [26, 48], and the hierarchical bucklings of an elastic charged ribbon [16]. Furthermore, fluctuations of surface charges in real systems may modify the bending rigidity and influence the stability of the charged membranes [13, 18, 49]. It is of great interest to generalize our model by including these effects to approach a real charged, deformable interface in the future work.

In summary, through the generalized Thomson problem, we study the combined effects of long-range interaction and curvature in shaping the crystalline order on the deformed sphere. As a key result in this work, we discover the depletion zone structure, and reveal its physical origin as a finite size effect that results from the geometry-regulated long-range interaction. These findings provide further insights into the crystallography of charged particles on curved surfaces. A future direction is to fully explore the shape space of a charged interface of various topologies. Notably, singularity structures may be developed over a freely evolving charged interface under the long-range interaction [26, 48].

Acknowledgement

Z.Y. and J.C. acknowledge support from NSFC Grant No.16Z103010253, the SJTU startup fund under Grant No.WF220441904, and the award of the Chinese Thousand Talents Program for Distinguished Young Scholars under Grants No.16Z127060004 and No. 17Z127060032. X.X. acknowledges support from NSFC via Grant No. 11674217, as well as Shanghai Municipal Education Commission and Shanghai Education Development Foundation via the ‘‘Shu Guang’’ project.

[1] L. Rayleigh, *Philos. Mag.* **14**, 184 (1882).

[2] D. Duft, H. Lebius, B. Huber, C. Guet, and T. Leisner,

Phys. Rev. Lett. **89**, 084503 (2002).

[3] Z. Liu, H. M. Wyss, A. Fernandez-Nieves, and H. C.

- Shum, *Phys. Fluids* **27**, 082003 (2015).
- [4] A. Huebner and H. Chu, *J. Fluid Mech.* **49**, 361 (1971).
- [5] J. Guerrero, J. Rivero, V. R. Gundabala, M. Perez-Saborid, and A. Fernandez-Nieves, *P. Natl. Acad. Sci. U.S.A.* **111**, 13763 (2014).
- [6] E. Pairem and A. Fernández-Nieves, *Phys. Rev. Lett.* **102**, 234501 (2009).
- [7] A. A. Fragkopoulos and A. Fernández-Nieves, *Phys. Rev. E* **95**, 033122 (2017).
- [8] A. Aggeli, I. A. Nyrkova, M. Bell, R. Harding, L. Carrick, T. C. McLeish, A. N. Semenov, and N. Boden, *P. Natl. Acad. Sci. U.S.A.* **98**, 11857 (2001).
- [9] A. S. Weingarten, R. V. Kazantsev, L. C. Palmer, M. McClendon, A. R. Koltonow, A. P. Samuel, D. J. Kiebal, M. R. Wasielewski, and S. I. Stupp, *Nat. Chem.* **6**, 964 (2014).
- [10] D. Andelman, *Handb. Biol. Phys.* **1**, 603 (1995).
- [11] R. Lipowsky and E. Sackmann, *Structure and Dynamics of Membranes*, vol. 1 (Elsevier, 1995).
- [12] S. Genet, R. Costalat, and J. Burger, *Biophys. J.* **81**, 2442 (2001).
- [13] Y. W. Kim and W. Sung, *Phys. Rev. Lett.* **91**, 118101 (2003).
- [14] G. Vernizzi and M. Olvera de la Cruz, *P. Natl. Acad. Sci. U.S.A.* **104**, 18382 (2007).
- [15] J. Adamcik, J.-M. Jung, J. Flakowski, P. De Los Rios, G. Dietler, and R. Mezzenga, *Nat. Nanotechnol.* **5**, 423 (2010).
- [16] Z. Yao and M. Olvera de la Cruz, *Phys. Rev. Lett.* **116**, 148101 (2016).
- [17] M. Winterhalter and W. Helfrich, *J. Phys. Chem.* **92**, 6865 (1988).
- [18] A. Lau and P. Pincus, *Phys. Rev. Lett.* **81**, 1338 (1998).
- [19] T. Nguyen, I. Rouzina, and B. Shklovskii, *Phys. Rev. E* **60**, 7032 (1999).
- [20] R. R. Netz, *Phys. Rev. E* **64**, 051401 (2001).
- [21] L. C. Palmer, Y. S. Velichko, M. Olvera de La Cruz, and S. I. Stupp, *Philos. T. Roy. Soc. A* **365**, 1417 (2007).
- [22] T. J. Moyer, H. Cui, and S. I. Stupp, *J. Phys. Chem. B* **117**, 4604 (2012).
- [23] G. Taylor, *Proc. R. Soc. London, Ser. A* **280**, 383 (1964).
- [24] A. Ziabicki, *Fundamentals of Fibre Formation: The Science of Fibre Spinning and Drawing* (John Wiley & Sons, New York, 1976).
- [25] A. G. Bailey, *Electrostatic Spraying of Liquids* (John Wiley & Sons, New York, 1988).
- [26] A. Gomez and K. Tang, *Phys. Fluids* **6**, 404 (1994).
- [27] M. Urbanski, C. G. Reyes, J. Noh, A. Sharma, Y. Geng, V. S. R. Jampani, and J. P. Lagerwall, *J. Phys.-Condens. Mat.* **29**, 133003 (2017).
- [28] J. J. Thomson, *Philos. Mag.* **7**, 237 (1904).
- [29] D. R. Nelson, *Defects and Geometry in Condensed Matter Physics* (Cambridge University Press, Cambridge, England, 2002).
- [30] J. De Luca, S. B. Rodrigues, and Y. Levin, *Europhys. Lett.* **71**, 84 (2005).
- [31] M. J. Bowick and L. Giomi, *Adv. Phys.* **58**, 449 (2009).
- [32] V. Koning and V. Vitelli, *Crystals and Liquid Crystals Confined to Curved Geometries* (John Wiley & Sons, Hoboken, 2016).
- [33] A. Bausch, M. Bowick, A. Cacciuto, A. Dinsmore, M. Hsu, D. Nelson, M. Nikolaides, A. Travasset, and D. Weitz, *Science* **299**, 1716 (2003).
- [34] G. Meng, J. Paulose, D. R. Nelson, and V. N. Manoharan, *Science* **343**, 634 (2014).
- [35] Z. Yao, *Soft Matter* **13**, 5905 (2017).
- [36] E. L. Altschuler, T. J. Williams, E. R. Ratner, R. Tipton, R. Stong, F. Dowl, and F. Wooten, *Phys. Rev. Lett.* **78**, 2681 (1997).
- [37] M. Bowick, A. Cacciuto, D. R. Nelson, and A. Travasset, *Phys. Rev. Lett.* **89**, 185502 (2002).
- [38] V. Vitelli, J. B. Lucks, and D. R. Nelson, *Proc. Natl. Acad. Sci. U.S.A.* **103**, 12323 (2006).
- [39] C. J. Burke, B. L. Mbang, Z. Wei, P. T. Spicer, and T. J. Atherton, *Soft Matter* **11**, 5872 (2015).
- [40] D. Mehta, J. Chen, D. Z. Chen, H. Kusumaatmaja, and D. J. Wales, *Phys. Rev. Lett.* **117**, 028301 (2016).
- [41] Z. Yao, *Soft Matter* **12**, 7020 (2016).
- [42] W. T. Irvine, V. Vitelli, and P. M. Chaikin, *Nature (London)* **468**, 947 (2010).
- [43] W. T. Irvine, M. J. Bowick, and P. M. Chaikin, *Nat. Mater.* **11**, 948 (2012).
- [44] D. Struik, *Lectures on Classical Differential Geometry* (Dover Publications, New York, 1988), 2nd ed.
- [45] W. Greub, S. Halperin, and R. Vanstone, *Lie Groups, Principal Bundles, and Characteristic Classes* (Academic Press, New York and London, 1973).
- [46] Z. Yao and M. Olvera de la Cruz, *Phys. Rev. Lett.* **111**, 115503 (2013).
- [47] A. Mughal and M. Moore, *Phys. Rev. E* **76**, 011606 (2007).
- [48] D. Duft, T. Achtzehn, R. Müller, B. A. Huber, and T. Leisner, *Nature (London)* **421**, 128 (2003).
- [49] Y. Kim and W. Sung, *Europhys. Lett.* **58**, 147 (2002).